Bulletin of Earthquake Engineering
https://doi.org/10.1007/s10518-026-02464-2

ORIGINAL ARTICLE

Numerical evaluation of hybrid reinforcement strategies for seismic enhancement of exterior RC beam–column joints

Mir Mahmoud Mousavizadeh[1] · **Elham Ghandi**[1]

Received: 17 December 2025 / Accepted: 3 April 2026

Abstract
This study presents a numerical investigation into the seismic performance of exterior reinforced concrete beam-column joints using LS-DYNA software, aiming to develop cost-effective reinforcement strategies that enhance ductility, energy dissipation, and post-earthquake reparability. Two hybrid reinforcement approaches are examined: (i) a shape memory alloy (SMA)–steel system for reducing residual drifts, and (ii) a novel dual-grade steel (DGS) configuration proposed as a practical alternative. A local weakening technique is introduced within the DGS system—achieved by splicing longitudinal bars of two distinct yield strengths—to intentionally shift the plastic hinge away from the joint core, thereby mitigating strain penetration and protecting the joint region. The finite element models are validated against experimental data. Parametric studies investigate (1) the effect of splice location in SMA–steel hybrid joints, revealing that a splice distance of 0.5 times the beam depth ($0.5h$) provides the most balanced performance; and (2) the seismic performance of the proposed DGS system. Results indicate that the DGS configuration achieves a 46% increase in cumulative energy dissipation and a 16% reduction in residual story drift compared to conventional steel-reinforced joints. Damage pattern analysis confirms successful relocation of the plastic hinge away from the joint core, promoting distributed inelasticity and enhanced repairability. The proposed DGS strategy offers a viable, cost-effective solution for resilient RC frame design, compatible with current construction practices.

Keywords Beam-column joints · Dual-grade steel (DGS) · Plastic hinge relocation · Seismic performance · LS-DYNA

✉ Elham Ghandi
ghandi@uma.ac.ir

[1] Department of Civil Engineering, Faculty of Technical and Engineering, University of Mohaghegh Ardabili, Ardabil, Iran

Published online: 21 April 2026

1 Introduction

Beam-to-column joints (BCJs) in reinforced concrete (RC) moment-resisting frames play a crucial role in controlling the seismic response of the entire structure. These joints are often considered the most vulnerable regions under strong ground motions because they are subjected to high shear stresses and complex force interactions. Damage localized within the joint core during severe earthquakes can significantly compromise the global stability of the structure, resulting in substantial strength degradation or, in extreme cases, collapse. Traditional seismic design philosophy aims to provide sufficient strength, stiffness, and ductility to ensure life safety; however, it does not necessarily guarantee post-earthquake functionality or ease of repair.

Following the devastating 1994 Northridge and 1995 Kobe earthquakes, which exposed severe limitations in conventional RC detailing and led to significant economic losses, the concept of low-damage and repairable design gained prominence. More recent seismic events—including the 2010–2011 Canterbury earthquakes in New Zealand (Fikri et al. 2019), the 2016 Central Italy earthquakes (Nascimbene 2024), and the 2023 Turkey-Syria earthquakes (Gurbuz and Cengiz 2025)—have further underscored the urgent need for structural systems that not only prevent collapse but also ensure post-earthquake functionality and repairability. These events have consistently demonstrated that economic losses and societal disruption can be significantly reduced through enhanced seismic resilience. Modern performance-based design approaches now emphasize not only collapse prevention but also rapid post-event recovery. Consequently, considerable research efforts have been directed toward developing self-centering and damage-controllable systems that can limit residual deformations and facilitate repair. Among the various emerging materials and technologies, shape memory alloys (SMAs) have attracted growing attention due to their unique superelastic and shape recovery properties. These alloys can undergo large reversible strains and return to their original configuration after unloading or upon heating, making them a promising solution for enhancing the seismic resilience and reparability of RC structures.

Parallel to material-based innovations, various structural techniques have been developed to protect the joint core by relocating the plastic hinge away from the column face. These approaches can be broadly categorized into two groups: (i) external or internal strengthening of joint, including the use of reinforced concrete jacketing (Karayannis et al. 2008), fiber-reinforced polymer (FRP) wrapping (Ilia and Mostofinejad 2019), enlarged joint panels (Tsonos 2005), additional straight-headed bars (Chutarat and Aboutaha 2003), additional 45° bent bars and 90° hooked bars (Hwang et al. 2015); and (ii) beam weakening strategies, such as reduced bar section (RBS) in RC joints (Mousavizadeh et al. 2024) and slotted beam (Oudah and El-Hacha 2017a). While these techniques have demonstrated varying degrees of success in protecting the joint region, they often involve significant construction complexity, added cost, or reliance on specialized materials. More recently, the use of superelastic shape memory alloy (SMA) bars has emerged as an effective method for both hinge relocation and residual drift reduction (Youssef et al. 2008; Alam et al. 2007), yet the high material cost of Ni-Ti SMAs remains a barrier to widespread implementation.

Numerous experimental studies have investigated the behavior of shape memory alloy (SMA) reinforcements in various reinforced concrete (RC) structural elements. Extensive research on beams has demonstrated the ability of SMA bars to enhance ductility and mitigate residual drifts (Ayoub 2003; Saiidi et al. 2007; Azadpour and Maghsoudi 2020;

Shrestha et al. 2013; Pareek et al. 2018; Abdulridha et al. 2013; Elbahy and Youssef 2019). Investigations on columns have similarly shown that the incorporation of SMA bars can significantly improve seismic resilience and energy dissipation (Saiidi and Wang 2006; Saiidi et al. 2009; Hosseini et al. 2015; Tazarv and Saiidi 2016). Experimental studies on shear walls confirmed the ability of SMA reinforcement to reduce residual deformations and confine damage within repairable limits (Hoult and de Almeida 2022a; Hoult and de Almeida 2022b; Abraik et al. 2020; Abdulridha and Palermo 2017; Tolou Kian and Cruz-Noguez 2018; de Almeida et al. 2020). Moreover, several researchers have explored RC beam–column joints incorporating SMA bars, reporting substantial improvements in joint re-centering capacity (Youssef et al. 2008; Alam et al. 2007; Nehdi et al. 2010; Qian et al. 2022; Oudah and El-Hacha 2017b, 2018, 2020).

Most of these studies have employed Nickel–Titanium (Ni–Ti) based SMAs, which exhibit a characteristic flag-shaped hysteretic response under cyclic loading. These alloys display higher compressive yield strength than tensile strength, resulting in an asymmetric stress–strain loop. The yielding of SMA corresponds to a reversible phase transformation between austenite and martensite phases (DesRoches et al. 2004).

Despite their outstanding self-centering capability and energy dissipation performance, the widespread application of SMAs in RC structures remains limited due to their relatively high cost. To address this limitation, several researchers have proposed hybrid reinforcement systems that combine SMA bars with conventional steel rebars. In these systems, SMA bars are strategically positioned in regions susceptible to plastic hinge formation, while conventional steel reinforcement is placed elsewhere. This hybrid configuration effectively reduces residual deformations after seismic events, thereby enhancing post-earthquake reparability and reducing repair costs (Kabir et al. 2016). Residual deformation, in this context, refers to the permanent displacement that remains after unloading once the applied stress has returned to zero.

2 Research significance

Hybrid reinforcement of RC beam–column joints using shape memory alloys (SMAs) in combination with conventional steel bars has gained significant attention due to its potential to reduce residual drifts and enhance post-earthquake reparability. However, despite these advantages, such systems exhibit two major limitations. First, the incorporation of SMA bars generally results in a reduction of initial stiffness because of their lower elastic modulus compared with conventional steel. Second, their energy dissipation capacity is inherently limited, as SMA materials typically display relatively narrow hysteresis loops under cyclic loading. These drawbacks highlight the necessity for alternative reinforcement solutions that can achieve similar or superior seismic performance while remaining economically viable.

As a first step, this study investigates the influence of splice location on the seismic performance of hybrid SMA–steel reinforced joints. While previous experimental research by Youssef et al. (2008) placed the SMA–steel splice within the joint core, the influence of splice location on seismic performance has not been systematically examined. Through a parametric finite element study using LS-DYNA, three different splice positions (0.25h, 0.5h, and 0.75h from the column face) are evaluated to identify the configuration that offers

the best balance between initial stiffness, energy dissipation capacity, and residual drift reduction. This investigation provides quantitative guidance for the design of SMA-based hybrid reinforcement systems.

Building upon the insights gained from the SMA splice study, the second and primary objective of this research is to introduce and evaluate a novel Dual-Grade Steel (DGS) system for plastic hinge relocation in RC beam-column joints. The concept of hinge relocation itself is well-established in steel structures through both strengthening and weakening techniques. However, in reinforced concrete construction, while joint strengthening techniques have been extensively studied, beam weakening strategies remain largely at a conceptual stage with limited systematic investigation (Mousavizadeh et al. 2024). The proposed DGS system addresses this gap by introducing a fundamentally new mechanical mechanism, namely local weakening via strength grading. Unlike SMA-based systems that rely on material superelasticity, the DGS system utilizes longitudinal reinforcement with two distinct yield strengths—lower-strength bars (400 MPa) placed near the joint and higher-strength bars (520 MPa) spliced beyond the intended hinge zone. This configuration creates a controlled flexural strength gradient along the beam length, effectively forming a plastic hinge away from the column face. The novelty lies in demonstrating that hinge relocation can be achieved through internal strength grading—a form of local weakening based on material strength differentiation—which has not been systematically investigated for RC beam-column joints prior to this study. Furthermore, the DGS system utilizes conventional steel grades and standard mechanical couplers already approved in construction codes, offering a practical and economical alternative to SMA-based systems.

3 Experimental database

In this research, the JBC1 and JBC2 specimens, which were previously tested by Youssef et al. (2008), were selected for validation in LS-DYNA using two concrete metrail models - Winfrith, and CDPM. The experimental program investigated the seismic behavior of BCJs reinforced with hybrid SMA and regular steel rebars. The specimens reported in the literature were designed and fabricated according to the requirements for moderate ductility level specified in CSA A23.3-04, as described by Youssef et al. (2008). It was subjected to cyclic loading up to a drift ratio of 7.9% to simulate severe earthquakes. The geometry and reinforcement details of the specimens are shown in Fig. 1. Specimen JBC1 is reinforced with regular steel bars, while JBC2 is reinforced with SMA bars in the plastic hinge region of the beam and ordinary steel bars in the rest of the joint.

The compressive strength of concrete at the time of testing was reported to be 53.5 MPa for specimen JBC-1 and 53.7 MPa for JBC-2. The corresponding splitting tensile strengths were 3.5 MPa and 2.8 MPa, respectively. For the 20 M reinforcing bars used in JBC-1, the yield strength, ultimate tensile strength, and Young's modulus were 520 MPa, 630 MPa, and 198 GPa. In contrast, the same properties for the 20 M bars in JBC-2 were 450 MPa, 650 MPa, and 193 GPa. In both specimens, 10 M steel bars were used for transverse reinforcement (ties), with a yield strength of 422 MPa and an ultimate strength of 682 MPa.

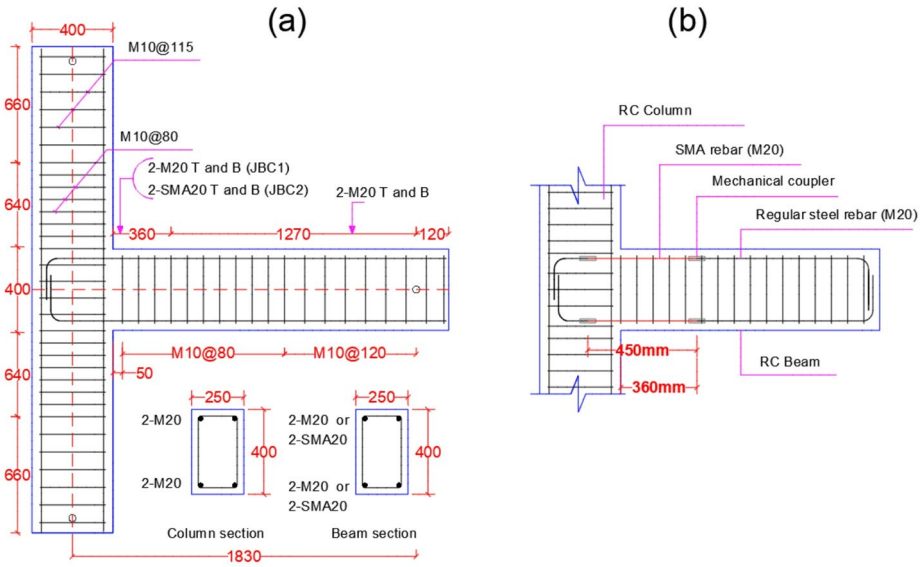

Fig. 1 (**a**) Geometry and reinforcement details of JBC1 and JBC2, (**b**) Splice details of specimen JBC2 (Youssef et al. 2008)

4 Methodology

Building upon the research significance outlined previously, this study develops a refined finite element modeling approach in LS-DYNA to quantitatively assess the proposed hybrid reinforcement strategies. The numerical framework focuses on accurately capturing the nonlinear cyclic response and damage progression in exterior RC beam-column joints. The Concrete Damage Plasticity Model (CDPM) is selected following a comprehensive evaluation against experimental benchmarks. The validated model is then employed in parametric studies to: (1) investigate the effect of splice location the splice location in hybrid SMA-steel systems for balanced seismic performance, and (2) evaluate the effectiveness of the novel Dual-Grade Steel (DGS) configuration as a practical alternative for plastic hinge relocation based on local weakening strategy.

4.1 Finite element modeling framework

Various theoretical frameworks have been developed to model the nonlinear behavior of concrete, including plasticity-based models, damage mechanics formulations, combined plasticity-damage approaches, and the total strain crack concept (Sarkis et al. 2022, 2023). In this study, considering the capabilities of LS-DYNA for seismic analysis of RC structures, two widely used concrete material models available in this platform—the Winfrith model (MAT084) and the Concrete Damage Plasticity Model (CDPM, MAT273)—were selected for comparative evaluation against experimental benchmarks. Both models have been extensively employed in numerical simulations of RC members under cyclic loading (Asgarpoor et al. 2021; Gharavi et al. 2022). As demonstrated in Sect. 5, CDPM exhibited superior accuracy in capturing the nonlinear cyclic behavior, damage patterns, and pinch-

ing response of RC beam-column joints. Therefore, CDPM was adopted for the subsequent parametric investigations.

4.1.1 Element types and material constitutive models

The concrete was modeled using 8-node hexahedral solid elements with reduced integration (ELFORM = 1) to enhance computational efficiency. This reduced integration technique is particularly effective in minimizing spurious energy modes, shear locking, and membrane locking, while also facilitating hourglass control (Nascimbene 2013). A known limitation of reduced integration schemes is the possible occurrence of hourglass modes, which may induce non-physical zero-energy deformations. To overcome this issue and ensure numerical stability, stiffness-based hourglass control (Type 5) was applied, following the recommendations of Hallquist (2006).

The steel reinforcement was modeled using the piecewise linear plasticity material model, which captures the elastic–plastic response of steel while accounting for strain-rate effects. Shape memory alloy (SMA) rebars were simulated using the MAT_SHAPE_MEMORY (MAT30) material model available in LS-DYNA. This uniaxial phenomenological model reproduces the essential features of SMA superelasticity, including asymmetric tension–compression behavior and the single-variant martensitic reorientation mechanism (Mohammadgholipour and Billah 2023). The input parameters for MAT30 were calibrated based on the experimental data reported by Youssef et al. (2008), as summarized in Table 1. The reinforcing bars were represented by one-dimensional Hughes–Liu beam elements, which can accurately simulate combined axial and flexural responses. A perfect bond between the concrete and reinforcement was assumed using the CONSTRAINED_LAGRANGE_IN_SOLID keyword. To simplify the numerical modeling, bar couplers were not explicitly included.

4.1.2 Loading protocol

The experimental program investigated the seismic behavior of BCJs reinforced with hybrid SMA and regular steel rebars. The lateral load was applied at the beam tip in two stages: (1) The first stage was force-controlled, with the loading continuing until the longitudinal reinforcing bars in the beam yielded. (2) The second stage switched to displacement control, with the loading continuing up to a 7.9% drift ratio. During the test, a constant axial load of 350 kN was applied at the top of the column.

Table 1 Mechanical properties of Ni-Ti SMA

Parameter	σ_s^{AS} (MPa)	σ_F^{AS} (MPa)	σ_s^{SA} (MPa)	σ_F^{AS} (MPa)	$\varepsilon_L(\%)$	E(GPa)
Value	401	520	370	130	6	62.5

Note. Data adapted from Youssef et al. (2008)

σ_s^{AS}: Austenite (A)-to-Martensite (M) starting stress, σ_F^{AS}: A-to-M finishing stress, σ_s^{SA}: M-to-A starting stress,σ_F^{AS}: M-to-A finishing stress,ε_L: recoverable strain and E: Young's modulus

Table 2 mesh specifications for sensitivity analysis

Model name	Concrete element size (mm)	Total number of solid elemnts	Concrete element type	Hourglass control type
Model 1	25 × 25 × 25 (whole model)	30,880	8-node Hexahedral (ELFORM = 1)	Type 5 (Stiffness-based)
Model 2	50 × 50 × 50 (whole model)	4000	8-node Hexahedral (ELFORM = 1)	Type 5 (Stiffness-based)
Model 3	25 × 25 × 25 (critical regions) 25 × 25 × 40 (remaining parts)	22,720	8-node Hexahedral (ELFORM = 1)	Type 5 (Stiffness-based)

4.2 Mesh-size effect

The mesh density was determined considering both the geometric characteristics of the specimen and computational efficiency. Although finer meshes generally provide higher numerical accuracy, they substantially increase the computational cost. Conversely, coarse meshes reduce the analysis time but may fail to capture local nonlinearities accurately. To evaluate the effect of mesh size on the cyclic response of the beam–column joint (BCJ), a mesh sensitivity study was performed using the Concrete Damage Plasticity Model (CDPM, MAT273). The experimental ultimate strength of specimen JBC1 (Youssef et al. 2008) was used as a reference for validation. Three finite element (FE) models with different mesh configurations were developed, as summarized in Table 2.

In all models, concrete was represented by 8-node hexahedral solid elements (ELFORM = 1) with stiffness-based hourglass control (Type 5) to suppress non-physical deformations. Model 1 employed a fine uniform mesh of 25 × 25 × 25 mm, resulting in 30,880 solid elements. Model 2 used a coarse uniform mesh of 50 × 50 × 50 mm, containing 4,000 elements. Model 3 implemented a graded mesh approach, applying finer elements (25 × 25 × 25 mm) in critical regions—such as the joint panel and load application zones—and slightly larger elements (25 × 25 × 40 mm) in less critical areas. This configuration produced 22,720 solid elements and achieved an effective balance between computational accuracy and efficiency.

The mesh configurations were evaluated based on the load–story drift hysteresis curves and ultimate strength values (as shown in Fig. 2; Table 3, respectively) under both positive and negative loading cycles.

Model 1 provided the closest agreement with experimental results but required significant computational resources. Model 2 overestimated the joint capacity, indicating its inability to capture localized nonlinear behavior accurately. Model 3 demonstrated the best trade-off, reproducing the nonlinear cyclic behavior with acceptable accuracy and manageable computational cost. Although Model 3 exhibits an 11.3% error in the negative direction, this level of accuracy is acceptable for comparative parametric studies. The experimental specimen itself exhibited asymmetric behavior, with ultimate strengths of 67.2 kN in the positive direction and 62.9 kN in the negative direction (see Table 3). When considering the average absolute error across both loading directions (7.66%), the model's performance is well within the typical range reported in validated numerical studies of RC joints. Furthermore, the model successfully reproduces the damage patterns (see Fig. 5) and overall hysteretic characteristics (see Fig. 4). Given the trade-off discussed above, Model 3 provides the most

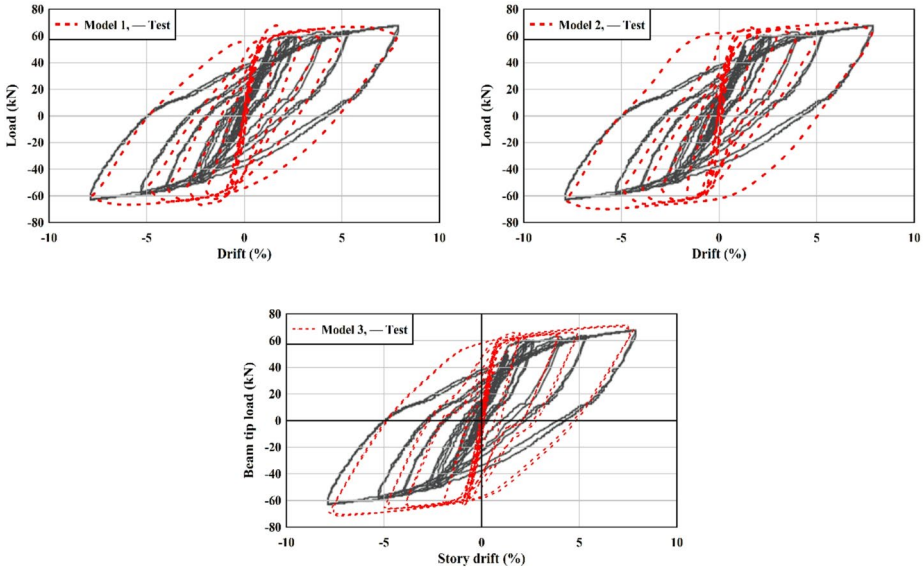

Fig. 2 effect of mesh size on hysteresis curve. Test result adapted from Youssef et al. (2008)

Table 3 Comparison of ultimate strength

Model	Ultimate Strength (kN) positivie direction	Ultimate Strength (kN) negative direction	Error (%) positivie direction	Error (%) negative direction
Test	67.2	62.9	-	-
Model 1	67.9	66.8	1.04	6.20
Model 2	71.5	71.7	6.41	13.97
Model 3	69.9	70	4.02	11.29

Note. Test data adapted from Youssef et al. (2008)

suitable balance between accuracy and computational demand for the extensive parametric investigations in this study. Therefore, Model 3 was adopted for subsequent analyses. The consistent application of this mesh configuration across all parametric models ensures that relative performance comparisons remain valid. The final FE model comprised 25,272 elements in total, including 2,552 beam elements and 22,720 solid elements, as illustrated in Fig. 3.

Although Model 3 exhibits an 11.3% error in the negative direction, this level of accuracy is considered acceptable for comparative parametric studies. It should be noted that the experimental specimen itself exhibited asymmetric behavior, with ultimate strengths of 67.2 kN in the positive direction and 62.9 kN in the negative direction (see Table 3). When considering the average absolute error across both loading directions (7.66%), the model's performance is well within the typical range reported in validated numerical studies of RC joints. Furthermore, the model successfully reproduces the damage patterns (see Fig. 5) and overall hysteretic characteristics (see Fig. 4). Given the trade-off discussed above, Model 3 provides the most suitable balance between accuracy and computational demand for the extensive parametric investigations in this study. The consistent application of this mesh

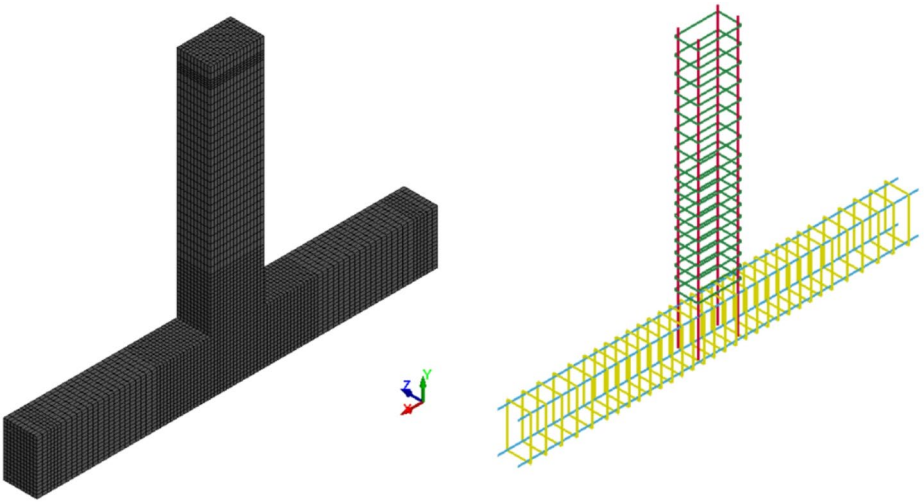

Fig. 3 Final FE model of specimen JBC1

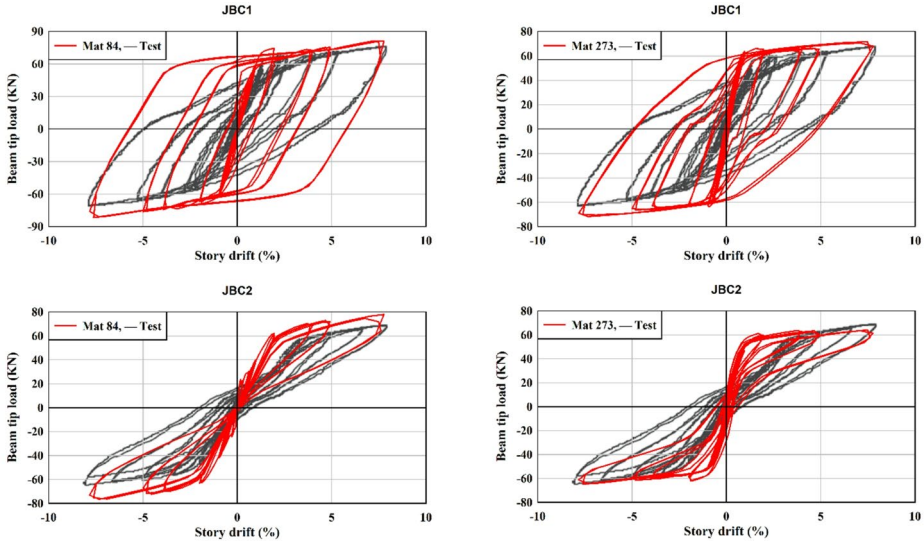

Fig. 4 Hysteresis response of tested specimens (Youssef et al. 2008) versus FE models

Table 4 Key parameters of BCJs hysteresis curve

Specimen	Result	Yielding strength		Ultimate strength		Energy	Residual story drift	$\frac{(P_u)_{FE}}{(P_u)_{test}}$
		δ_y (mm)	P_y (kN)	δ_u (mm)	P_u (kN)	E (kN.m)	(%)	
JBC1	Test	12	51.3	72	67.2	26.5	4.94	-
	Mat 84	13.9	67.2	72	81.1	57.4	5.79	1.22
	Mat 273	10.3	58.5	72	69.9	42.6	4.69	1.07
JBC2	Test	18	32.7	72	68.3	16.7	1.98	-
	Mat 84	21.8	64.4	72	77.8	13.2	0.17	1.14
	Mat 273	14.4	52.4	72	64.1	12.6	0.35	0.94

Note. Test results adapted from Youssef et al. (2008)

configuration across all parametric models ensures that relative performance comparisons remain valid.

5 FE results and discussion

To ensure the reliability of the numerical results for parametric investigation, the modeling approach was rigorously validated against the cyclic test data of specimens JBC1 and JBC2 reported by Youssef et al. (2008). The validation process involved comparing numerical predictions with experimental results in terms of hysteresis response, damage patterns, and key seismic performance parameters including yielding strength, ultimate strength, energy dissipation capacity, and residual story drift.

5.1 Hysteresis load-displacement curves

The test results (Youssef et al. 2008) indicated that the specimens did not experience a significant reduction in strength. The specimen JBC2 experienced more pinching and the flag-shape response of SMA dominated the cyclic behavior of the joint. Figure 4 compares the beam tip load-story drift hysteretic curves of models with the test results. Table 4 reports the key parameters of the hysteretic curves, including yielding and ultimate strength, cumulative energy dissipation capacity at a story drift ratio of 7.9%, and residual story drift.

For most parameters listed in Table 4, the CDPM model demonstrated higher predictive accuracy than the Winfrith model for both specimens. In particular, CDPM achieved an error of less than 7% in predicting the ultimate load for each specimen, indicating superior performance in capturing peak strength behavior. Specimen JBC2 exhibited characteristic pinching behavior in its hysteresis response, attributed to the superelastic nature of SMA. Both the CDPM and Winfrith models successfully reproduced this pinching effect, despite not explicitly incorporating bond–slip mechanisms between reinforcement and concrete. However, the Winfrith model, which accounts for crack opening and closing, tended to overestimate the extent of pinching compared to the experimental observations.

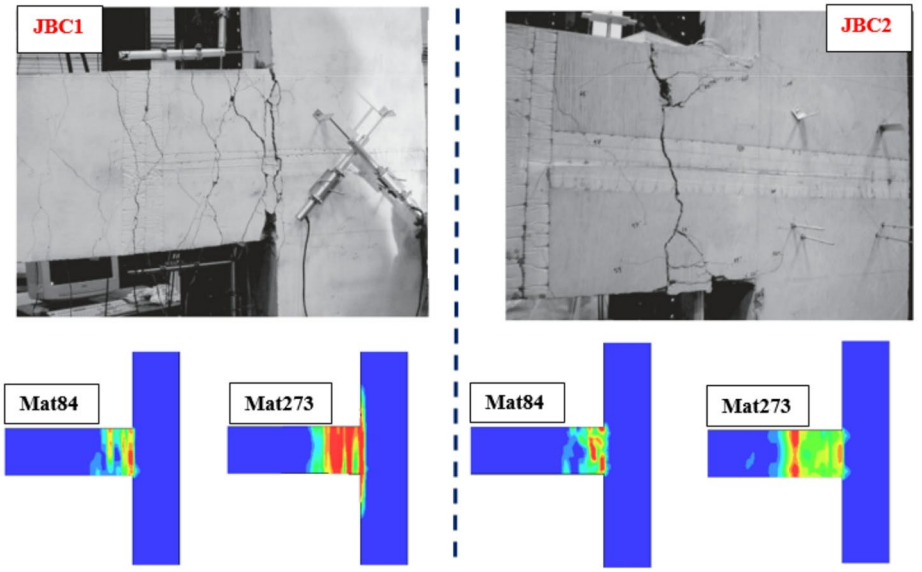

Fig. 5 Comparison of observed (Youssef et al. 2008) and predicted damage patterns at 7.9% drift ratio

5.2 Damage and cracking pattern

Figure 5 compares the observed damage patterns from the experimental tests with the numerical predictions at a 7.9% drift ratio. In the simulations, the maximum principal strain was adopted as the criterion for identifying concrete damage, following the approach outlined in (Gharavi et al. 2022; Asgarpoor et al. 2021).

The experimental results showed ductile behavior, consistent with the performance expectations of the CSA A23.3-04 design code, with most observed cracks in the beams classified as flexural cracks. In specimen JBC1, a plastic hinge formed at the column face, whereas in JBC2, the use of superelastic SMA bars successfully relocated the plastic hinge away from the joint core.

As illustrated in Fig. 5, the Winfrith model produced similar damage distributions for both specimens, failing to distinguish between their distinct behaviors. In contrast, the CDPM model accurately predicted the location and extent of cracking and damage zones, successfully capturing the differences in damage progression between JBC1 and JBC2.

Based on both the load–displacement response and the damage pattern predictions, the CDPM model demonstrated superior accuracy in simulating the cyclic behavior of beam–column joints (BCJs). Consequently, it was selected for use in the subsequent parametric analyses.

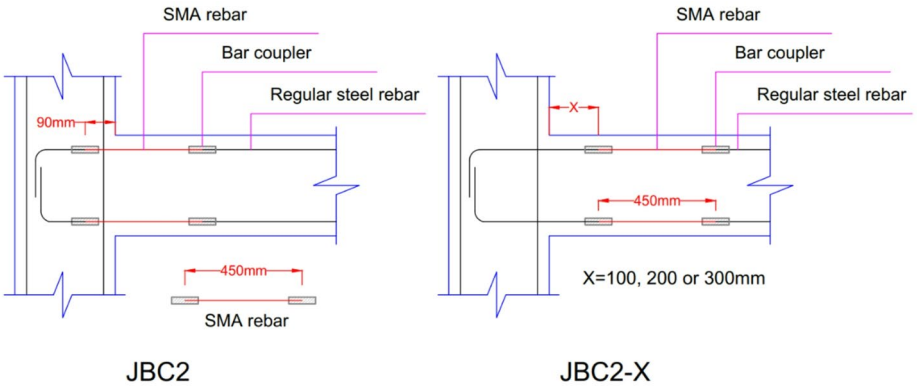

Fig. 6 Longitudinal reinforcement layout of the reference specimen JBC2 and the proposed models JBC2-X

6 Parametric investigation of hybrid SMA–steel reinforcement through splice relocation

The primary advantage of incorporating superelastic SMAs in specimen JBC2 lies in the significant reduction of residual story drift following cyclic loading, as well as the relocation of the plastic hinge away from the column face. However, this configuration also exhibited certain limitations, including reduced initial stiffness and limited energy dissipation capacity when compared to the conventional steel-reinforced specimen JBC1. To address these shortcomings, a numerical study was conducted to enhance the seismic performance of the SMA-based system.

In specimen JBC2, the SMA–steel splice was placed within the joint core, at a distance of 90 mm from the column face. In the improved configurations, the splice location was shifted outside the joint core to evaluate its influence on seismic performance. The numerical models are labeled JBC2-X, where X represents the splice distance (in millimeters) from the column face. As illustrated in Fig. 6, three splice locations—0.25h (100 mm), 0.5h (200 mm), and 0.75h (300 mm), where h is the beam depth—were examined. The objective was to identify the optimal splice location that enhances initial stiffness and energy dissipation while maintaining acceptable residual drift and minimizing concentrated damage.

The selected splice locations—0.25h, 0.5h, and 0.75h from the column face—were chosen to cover the practically feasible range for plastic hinge relocation in RC beams. Locations closer than 0.25h would place the splice too near the joint core, providing minimal benefit in terms of hinge relocation and damage distribution. Conversely, locations beyond 0.75h would reduce the effective shear span, potentially leading to excessive curvature and shear demands that could accelerate degradation and alter the expected failure mechanism. Therefore, the investigated range represents the mechanically meaningful domain for splice relocation, within which three discrete positions were examined to identify the most balanced configuration.

The cyclic responses of the joints for different splice configurations as well as damage paterns are presented in Fig. 7, and a summary of key performance indicators, including stiffness, energy dissipation, and residual drift, is provided in Table 5.

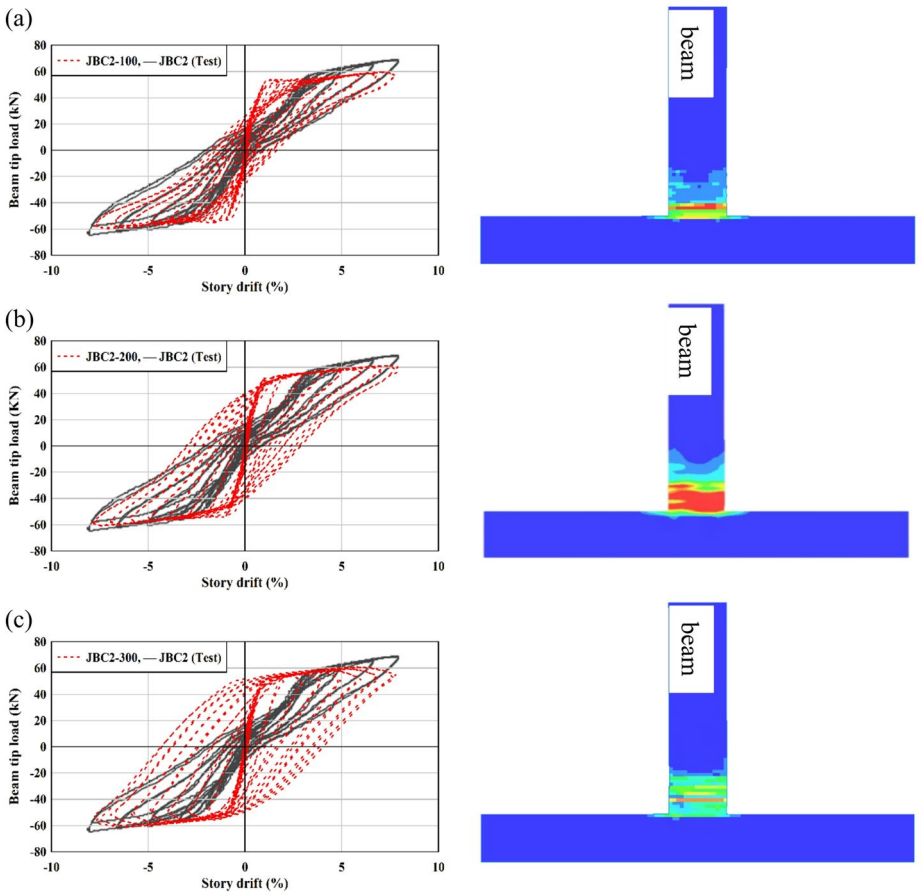

Fig. 7 Hysteresis curves and final damage patterns of the proposed hybrid SMA–steel reinforcement, (**a**) JBC2-100, (**b**) JBC2-200, and (**c**) JBC2-300. Test data adapted from Youssef et al. (2008)

Table 5 Summary of seismic performance indicators for numerical models

Result	JBC2	JBC2-100	JBC2-200	JBC2-300
Ultimate strength P_u (kN)	68.3	59.7	61.4	60.8
Dissipated Energy E (kN.m)	16.7	29.9	47.7	64.0
Initial stiffness K_i (kN/mm)	7.5	8.62	8.94	8.63
Residual story drift R_d (%)	1.98	1.65	2.89	3.93

Note. Test results for JBC2 adapted from Youssef et al. (2008)

Notably, all three proposed models outperformed the experimental specimen JBC2 in terms of both initial stiffness and energy dissipation capacity, indicating that relocating the splice outside the joint panel enhances seismic resilience. To ensure consistent comparison, the initial stiffness was calculated using the force–displacement response up to the point of

first flexural cracking in the beam. This pre-cracking secant stiffness represents the elastic response of the uncracked section and provides a physically meaningful basis for comparing different reinforcement configurations. Based on the experimental data reported by Youssef et al. (2008), first flexural cracking occurred at a drift ratio of approximately 0.22%. Accordingly, the secant stiffness was determined by dividing the lateral load by the corresponding lateral displacement at this drift level. The same drift level was applied uniformly across all models, ensuring that relative performance trends remain valid.

Among the proposed configurations, the JBC2-300 model (splice at 0.75*h*) dissipated the most energy (64.0 kN·m) and exhibited broad hysteresis loops, reflecting increased ductility due to a more distributed plastic hinge. However, it also experienced the highest residual drift (3.93%) and more widespread damage along the beam, which could affect reparability and functionality after seismic events. In contrast, JBC2-100 (splice at 0.25*h*) demonstrated a relatively stiff and elastic behavior with the lowest residual drift (1.65%) and reduced damage propagation. However, its energy dissipation capacity was more limited (29.9 kN·m).

The intermediate model, JBC2-200 (splice at 0.5*h*), offered the most balanced performance, achieving the highest initial stiffness (8.94 kN/mm), substantial energy dissipation (47.7 kN·m), and moderate residual drift (2.89%), along with a favorable and stable damage pattern.

While relocating the splice away from the joint panel improves energy dissipation and inelastic deformation capacity, excessive offset distances may reduce the effective shear span. This can increase curvature and shear demand at the relocated plastic hinge, potentially leading to accelerated degradation. As hypothesized and confirmed through this parametric study, increasing the splice distance beyond 0.75*h* could negatively affect joint performance. Therefore, placing the splice at approximately 0.5*h* from the column face is recommended as the most balanced configuration among the three locations investigated (0.25*h*, 0.5*h*, and 0.75*h*), effectively balancing strength, stiffness, ductility, and post-earthquake reparability within the mechanically meaningful range examined.

7 Hybrid reinforcement strategy using dual-grade steel (DGS) bars

One of the primary challenges in the practical implementation of SMA-based reinforcement systems is their high material cost, which significantly limits widespread adoption in real-world structures (Youssef et al. 2008). Additionally, in RC moment-resisting frames designed based on the weak beam–strong column philosophy, plastic hinges are expected to form within the beam spans. However, experimental observations indicate that strain penetration often extends into the joint core beyond the yield limit, resulting in undesirable failure modes and compromising the seismic resilience of BCJs (Rutledge et al. 2014). Studies have revealed that cracking may initiate within the joint panel even before full plastic hinge development in the beam, with these cracks propagating more severely once the longitudinal reinforcement yields. This behavior leads to premature bond degradation, increased damage to the core concrete, and deviation from the idealized rigid joint assumption commonly used in structural analysis models (Tsonos 2005). To address these challenges, relocating the plastic hinge away from the column face has been proposed as an effective strategy, as it mitigates strain penetration and delays concrete degradation within the joint region (Chutarat and Aboutaha 2003).

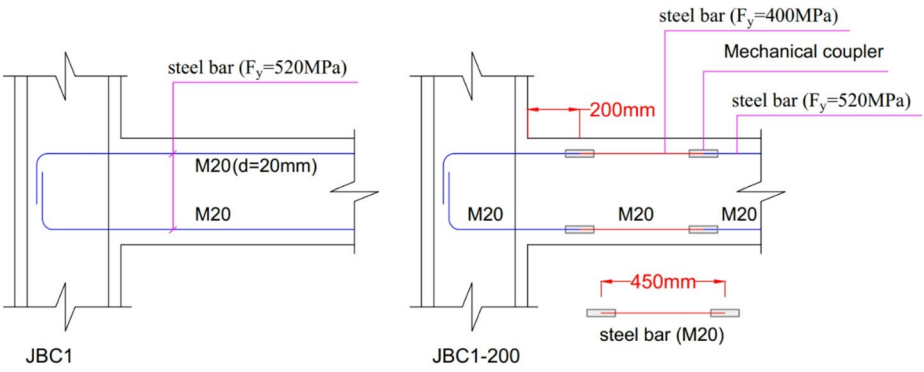

Fig. 8 Longitudnal reinforcement details of specimens JBC1 (Youssef et al. 2008) and the proposed DGS system

Although local weakening strategies have been effectively implemented in steel moment-resisting frames to relocate plastic hinges, their application in RC beam–column joints remains limited and is mostly at a conceptual stage. A recent experimental study by Mousavizadeh et al. (2024) confirmed the feasibility of this approach for RC structures using two specific techniques: (i) reduction of bar cross-sectional area (RBS), and (ii) reduction of the beam's effective depth (RED). Among these, the RBS technique exhibited better seismic performance by significantly improving energy dissipation and ductility (achieving drift ratios up to 3.5%), while also mitigating pinching behavior and suppressing diagonal cracking within the joint core.

Motivated by these promising findings and the need for a more practical and economical solution, the present study explores an alternative strategy that achieves similar hinge relocation effects without relying on costly or complex modifications.

Building on the favorable performance of the hybrid SMA–steel reinforcement observed in the JBC2 specimen and its numerical extensions (JBC2-100, 200, 300), this section introduces a cost-effective alternative: Dual-Grade Steel (DGS) reinforcement. This approach involves the use of longitudinal reinforcement with two distinct yield strengths within the beam, enabling intentional redistribution of flexural strength to create a localized weak zone away from the joint core. As a result, plastic hinge formation is encouraged at a safer distance from the column face. Importantly, the proposed DGS strategy is both practical and economical, as it employs conventional steel reinforcement grades and standard mechanical couplers that are readily available in current construction practice.

7.1 Details of proposed BCJ with DGS bars

Figure 8 illustrates the longitudinal reinforcement layout of the reference specimen JBC1 (Youssef et al. 2008) and the proposed DGS-integrated specimen JBC1-200. Both specimens share identical geometry and transverse reinforcement configurations. The key modification in JBC1-200 lies in the use of Dual-Grade Steel (DGS) in the beam's longitudinal reinforcement.

In the JBC1-200 specimen, longitudinal bars with a yield strength of 400 MPa are spliced to higher-strength bars (520 MPa) using mechanical couplers located 200 mm away

from the column face. This specific distance was selected based on the favorable behavior observed in the JBC2-200 model, where relocating the splice farther from the joint core led to optimum seismic behavior of SMA-based joints. This reverse-grade splicing—placing the lower-strength bars nearer to the joint—creates a controlled reduction in flexural capacity outside the joint core. Consequently, the plastic hinge is expected to form at the intended splice location, safely away from the column face.

The 450 mm length of the lower-strength (400 MPa) bars beyond the splice point in the proposed DGS model was inspired by the reinforcement detailing of the JBC2 specimen, experimentally tested by Youssef et al. (2008). This length was originally selected in JBC2 based on the estimated plastic hinge length (360 mm) and the location of the splice, which started 90 mm inside the joint core. The similar bar length is adopted in the current model to maintain consistency with the detailing used in JBC2. However, in contrast to the SMA-based strategy of JBC2, the present study aims to relocate the plastic hinge through local flexural weakening by employing longitudinal steel bars with two different yield strengths.

It is important to note that the 450 mm length is not a fixed requirement in the DGS configuration; rather, its value may be further investigated through parametric sensitivity analysis in future studies, as long as effective hinge relocation and flexural redistribution are ensured. Ultimately, the performance of the proposed DGS system is evaluated by direct comparison with the reference specimen JBC1, also tested by Youssef et al. (2008), to assess its viability as a practical and economical alternative for enhancing seismic performance in RC beam–column joints.

While a detailed cost analysis is beyond the scope of this numerical study, the proposed DGS system offers potential practical advantages compared to SMA-based alternatives. The reinforcing bars used (400 MPa and 520 MPa yield strengths) are standard grades widely available in many countries and conform to common construction codes such as ACI 318−19 (ACI 2019). The mechanical couplers required for splicing are also commercially available and routinely used in practice. From a constructability perspective, the DGS configuration does not require specialized fabrication or geometric modification of bars, unlike reduced bar section (RBS) techniques (Mousavizadeh et al. 2024). These factors suggest that the DGS system could be implemented with minimal additional cost compared to conventional reinforcement, while avoiding the high material costs associated with Ni-Ti SMAs. Furthermore, by utilizing conventional steel rather than energy-intensive shape memory alloys, the DGS approach may offer environmental benefits in terms of embedded carbon, as demonstrated in comparative life-cycle assessments of traditional versus dissipation-based retrofitting solutions (Cavalieri et al. 2023). However, comprehensive cost-benefit and life-cycle assessment studies are needed to quantify these potential advantages.

7.2 Seismic responses

Given that the numerical modeling techniques - including element types and material models - are consistent with those detailed in Sect. 4, this section focuses on the seismic responses of the proposed DGS model (JBC1-200) and its comparison with the experimental benchmark specimen JBC1.

Figure 9a shows the beam tip load versus story drift hysteresis curves for both specimens. The peak lateral strength of JBC1-200 is nearly identical to that of the reference specimen, indicating that the introduction of Dual-Grade Steel (DGS) reinforcement does not com-

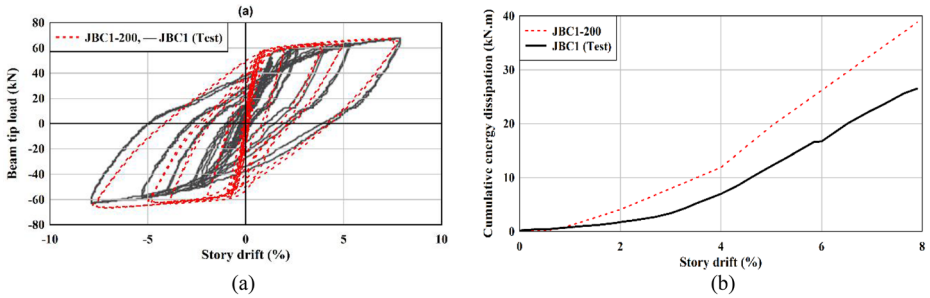

Fig. 9 (**a**) Hysteresis curves of JBC1 (Youssef et al. 2008) and JBC1-200, (**b**) Cumulative energy dissipation cappacity

promise the global load-carrying capacity. However, the DGS model exhibits significantly improved deformation characteristics. Specifically, it achieves a maximum residual drift of 4.15%, which is approximately 16% lower than that of JBC1. This reduction suggests better post-cyclic recentering behavior and lower permanent deformation, which are desirable for minimizing residual damage after seismic events.

Figure 9b compares the cumulative energy dissipation of the two specimens. At a story drift of 7.9%, the DGS model dissipates 38.8 kN·m, whereas the reference specimen dissipates only 26.5 kN·m. This corresponds to a 46% enhancement in energy absorption capacity, primarily due to the more distributed plasticity and reduced damage concentration near the joint core. The DGS configuration promotes yielding away from the column face by exploiting the intentional flexural weakness introduced at the grade transition location, thus enabling the formation of multiple stable hysteresis loops with reduced strength degradation.

To provide a more complete interpretation of the enhanced energy dissipation observed in the DGS specimen, Fig. 10 presents the backbone curves and stiffness degradation trends for both JBC1 and JBC1-200. All response quantities are extracted from the first cycle of loading, which represents the structure's behavior upon first reaching a given deformation level. Figure 10a shows the envelope of peak loads (skeleton curves) throughout the loading history. Figure 10b displays the secant stiffness degradation, where stiffness at each drift level is calculated from the first cycle response.

The envelope of peak loads shows that JBC1 reaches its ultimate strength of 67.2 kN at 7.9% drift, while JBC1-200 achieves 65.33 kN at the same drift level. Although the reference specimen exhibits slightly higher peak load, the DGS specimen maintains a more gradual strength gain beyond 4% drift, indicating stable inelastic behavior without premature degradation. At 7.9% drift, both specimens reach their peak strength. This confirms that the 46% increase in energy dissipation in the DGS system is achieved without any reduction in peak strength.

It should be noted that Youssef et al. (2008) did not report stiffness degradation for JBC1. Therefore, for comparative purposes, stiffness values for JBC1 are derived from the validated numerical model (Model 3), which demonstrated good agreement with experimental results, as shown in Figs. 4 and 5. Both specimens exhibit similar initial stiffness. Up to 4% drift, JBC1 exhibits slightly higher stiffness compared to JBC1-200. Beyond 4% drift, the stiffness values of both specimens become nearly identical, with JBC1-200 showing com-

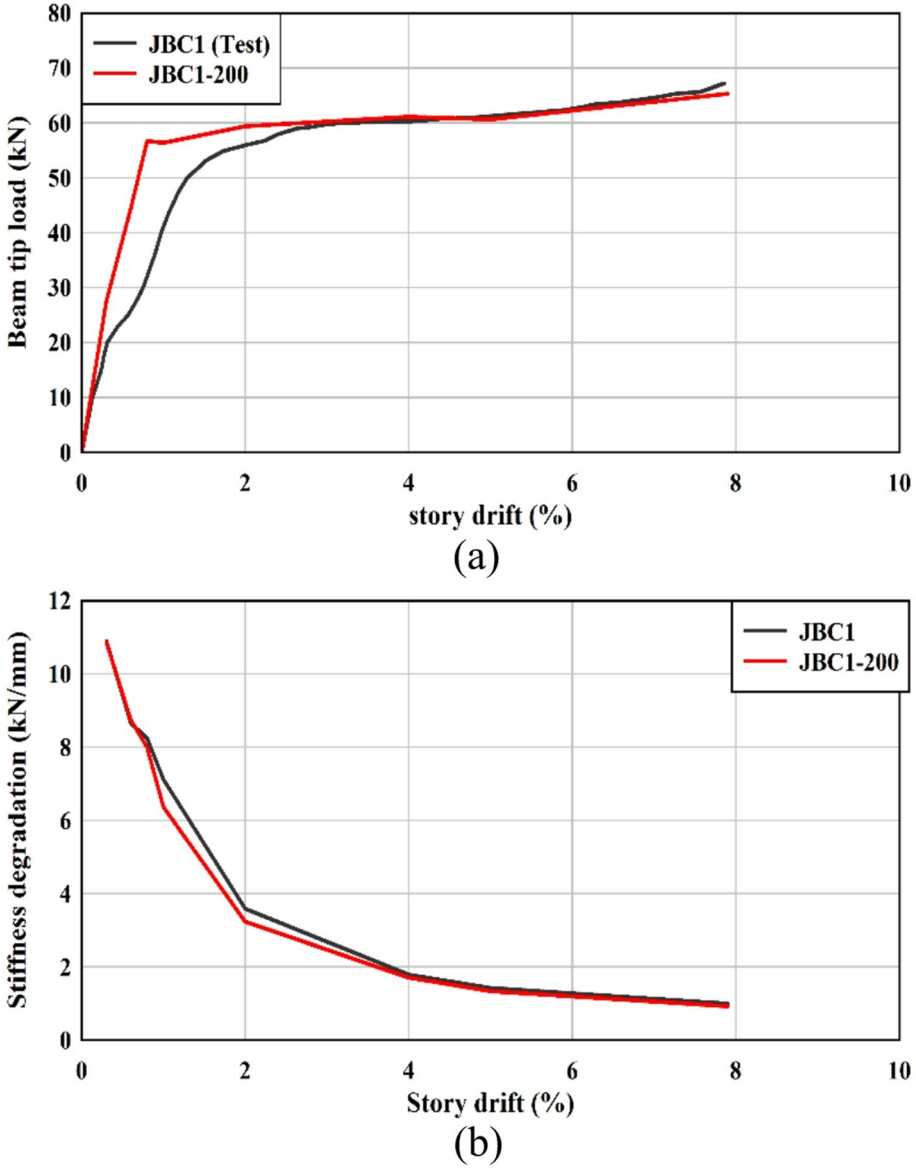

Fig. 10 Seismic performance indicators for JBC1 and JBC1-200, (**a**) Backbone curves and, (**b**) Stiffness degradation

parable performance up to 7.9% drift. This indicates that the enhanced energy dissipation of the DGS system is achieved without accelerated stiffness degradation.

These seismic indicators collectively confirm that the DGS system not only enhances energy dissipation but also maintains stable strength and stiffness throughout the loading history, validating its seismic resilience without premature degradation.

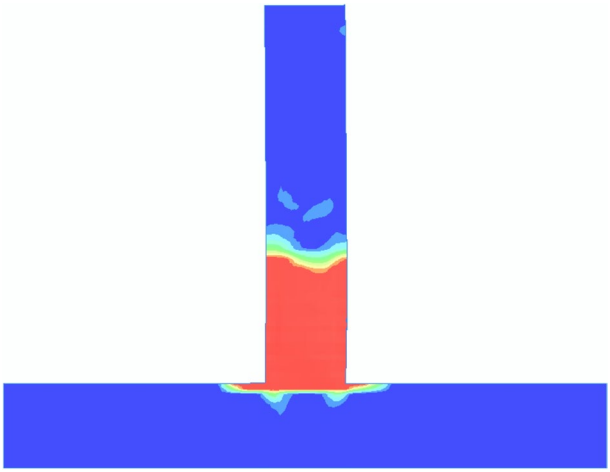

Fig. 11 Damage pattern of specimen JBC1-200

Figure 11 depicts the simulated damage distribution in specimen JBC1-200 at peak story drift. The damage contours reveal that the plastic hinge region has successfully shifted away from the column face and is now located near the splice point, consistent with the design intent of the DGS configuration. Unlike the reference specimen, where high concentrations of strain and damage are typically observed at the beam–column interface (see Fig. 5), here the inelastic zone has broadened along the beam length.

The reduced concentration of red/yellow damage contours near the joint core also suggests a mitigation of diagonal shear cracking, which is often associated with brittle failure modes in conventional RC joints. In contrast, the DGS specimen exhibits a more ductile damage evolution, with increased tensile cracking in the beam region rather than the joint. This controlled relocation of plasticity not only protects the integrity of the column face but also contributes to improved cumulative energy dissipation, as discussed earlier.

These numerical results validate the hypothesis that introducing local flexural weakening through dual-grade reinforcement effectively relocates the plastic hinge, reduces residual drift, and enhances energy dissipation—without negatively affecting peak strength.

To provide a mechanics-based justification for the reduced diagonal cracking observed in Fig. 11, the joint shear demand and nominal shear capacity were evaluated for both specimens. The shear demand was calculated using the relation proposed by Mousavizadeh et al. (2024) for external joints incorporating plastic hinge relocation:

$$V_{ju} \cong \alpha \left(\frac{M_n l_s}{l_s - d_j} \right) \times \frac{1}{h_s} - V_{col}, \ and \ V_{col} = P_u \frac{l}{h} \tag{1}$$

where M_n is the moment capacity at the critical section of the beam, $l_s$is distance from the joint face to the loading point ($l_s = 1630mm$), $d_j$is the distance from the critical section to the joint face (taken as zero for specimens without hinge relocation and 200 mm for JBC1-200), $h_s$is the distance between the top and bottom longitudinal bars of the beam ($h_s = 320mm$), V_{col} is the column shear force determined from equilibrium, P_u is the ultimate lateral strength of the joint, l is the distance from the joint center to the loading point on the beam tip ($l = 1830mm$), and h is the net height of the column between supports

Table 6 Joint shear demand and capacity comparison

Specimen	V_{ju} Eq. (1)	V_n Eq. (2)	$\frac{V_{ju}}{V_n}$
JBC1	500.4	731.4	0.68
JBC1-200	440.4	731.4	0.60

($h = 2740mm$). The parameter α accounts for the over-strength due to strain hardening of the longitudinal reinforcement. In accordance with ACI 318−19 (Section 18.8.2.1), the value of α is taken as 1.25 for all calculations in this study.

The nominal shear capacity of the joint was determined according to ACI 318−19 (ACI 2019) provisions for exterior joints:

$$V_n = \sqrt{f'_c}\,\mathrm{h_c b_j} \tag{2}$$

where $f'_c = 53.5MPa$ is the concrete compressive strength, $b_j = 250mm$ is the effective joint width (taken as the column width), and $h_c = 400mm$ is the column depth in the direction of shear.

Based on the relations presented above, the joint shear demand for the reference specimen JBC1 was calculated as 500.4 kN, while for the proposed DGS specimen JBC1-200 it was 440.4 kN. The nominal shear capacity, determined from Eq. (2), is 731.4 kN for both specimens. A summary of the shear demand-capacity analysis is presented in Table 6.

For JBC1, the shear demand reaches approximately 68% of the capacity, indicating that the joint is critically stressed. In contrast, for the proposed DGS specimen JBC1-200, the shear demand is reduced to 60% of the capacity. This 12% reduction in demand-capacity ratio is attributed to the relocation of the plastic hinge away from the column face, which limits strain penetration into the joint core and reduces the tensile forces transferred to the joint region. The lower shear demand provides a clear mechanics-based explanation for the reduced diagonal cracking observed in Fig. 11.

8 Conclusion

This study numerically assessed the seismic performance of RC beam-to-column joints using two advanced hybrid reinforcement strategies: SMA–steel combinations and a newly proposed dual-grade steel (DGS) configuration. Key conclusions are summarized below:

1. Among the two concrete models evaluated, the CDPM (MAT273) model demonstrated superior accuracy in simulating nonlinear cyclic behavior, including cracking, pinching, and damage propagation, making it suitable for parametric analyses of RC joints.
2. Relocating the SMA–steel splice outside the joint panel substantially improved the initial stiffness and energy dissipation of the hybrid joint, while only slightly increasing residual story drift. A splice location at 0.5*h* from the column face offered the best balance of strength, ductility, and reparability.
3. The DGS reinforcement strategy, utilizing longitudinal bars of two different yield strengths, successfully created a localized plastic hinge away from the joint core. This method achieved a 46% increase in energy dissipation and 16% reduction in residual drift compared to the conventional RC joint, without sacrificing peak lateral strength.

4. The local weakening technique proposed herein is practical, cost-effective, and compatible with current construction practices, eliminating the need for expensive smart materials like SMA.
5. A mechanics-based shear demand-capacity analysis was conducted to justify the observed reduction in joint diagonal cracking. The results showed that the proposed DGS system reduces the joint shear demand from 68% to 60% of the nominal capacity, corresponding to a 12% decrease in the demand-capacity ratio. This reduction is attributed to the relocation of the plastic hinge away from the column face, which limits strain penetration into the joint core and alleviates shear stresses in the joint region. The quantitative shear assessment confirms that the DGS configuration not only enhances energy dissipation but also provides improved protection against joint shear failure.
6. The limitations of the perfect bond assumption should be acknowledged. While the numerical models accurately captured damage patterns and overall hysteretic response (Figs. 4 and 5), the 82% error in residual drift prediction for JBC2 indicates that absolute residual displacements should be interpreted with caution. The reported improvements for the DGS system (46% energy increase, 16% drift reduction) are numerical predictions requiring experimental validation. Future work should include full-scale experimental testing of the DGS system and incorporation of advanced bond-slip models to refine localized damage predictions.

Author contributions CRediT taxonomy: Conceptualization: Mir Mahmoud Mousavizadeh, Elham Ghandi; Methodology: Mir Mahmoud Mousavizadeh; Software: Mir Mahmoud Mousavizadeh; Formal Analysis and investigation: Mir Mahmoud Mousavizadeh ; Writing – Original Draft: Mir Mahmoud Mousavizadeh; Writing - review and editing: Elham Ghandi; Resources: Elham Ghandi; Supervision: Elham Ghandi.

Funding The authors declare that no funds, grants, or other support were received during the preparation of this manuscript.

Data availability The datasets generated during and/or analysed during the current study are available from the corresponding author on reasonable request.

Declarations

AI assisted copy editing The authors used an AI-based language editing tool (Monica) to assist in improving the readability and linguistic clarity of the manuscript. The authors are solely responsible for the final version of the text.

Competing interests The authors have no relevant financial or non-financial interests to disclose.

References

Abdulridha A, Palermo D (2017) Behaviour and modelling of hybrid SMA–steel reinforced concrete slender shear wall. Eng Struct 147:77–89. https://doi.org/10.1016/j.engstruct.2017.04.058

Abdulridha A, Palermo D, Foo S, Vecchio FJ (2013) Behavior and modeling of superelastic shape memory alloy reinforced concrete beams. Eng Struct 49:893–904. https://doi.org/10.1016/j.engstruct.2012.12.041

Abraik E, El-Fitiany SF, Youssef MA (2020) Seismic performance of concrete core walls reinforced with shape memory alloy bars. Structures 27:1479–1489. https://doi.org/10.1016/j.istruc.2020.07.053

ACI (2019) ACI 318 – 19: Building Code Requirements for Structural Concrete and Commentary. American Concrete Institute, Farmington Hills, MI

Alam MS, Youssef MA, Nehdi M (2007) Seismic behaviour of concrete beam–column joints reinforced with superelastic shape memory alloys. In: 9th Canadian Conference on Earthquake Engineering, Ottawa, Canada p 10

Asgarpoor M, Gharavi A, Epackachi S (2021) Investigation of various concrete materials to simulate seismic response of RC structures. Structures 29:1322–1351. https://doi.org/10.1016/j.istruc.2020.11.042

Ayoub CA (2003) A study of shape-memory-alloy reinforced beams and cubes. PhD Dissertation, University of Nevada, Reno, USA

Azadpour F, Maghsoudi AA (2020) Experimental and analytical investigation of continuous RC beams strengthened by SMA strands under cyclic loading. Constr Build Mater 239:117730. https://doi.org/10.1016/j.conbuildmat.2019.117730

Cavalieri F, Bellotti D, Caruso M, Nascimbene R (2023) Comparative evaluation of seismic performance and environmental impact of traditional and dissipation-based retrofitting solutions for precast structures. J Build Eng 79:107918. https://doi.org/10.1016/j.jobe.2023.107918

Chutarat N, Aboutaha RS (2003) Cyclic response of exterior reinforced concrete beam–column joints reinforced with headed bars—experimental investigation. ACI Struct J 100(2):259–264. https://doi.org/10.14359/12490

de Almeida JP, Steinmetz M, Rigot F, de Cock S (2020) Shape-memory NiTi alloy rebars in flexural-controlled large-scale reinforced concrete walls: experimental investigation on self-centring and damage limitation. Eng Struct 220:110865. https://doi.org/10.1016/j.engstruct.2020.110865

DesRoches R, McCormick J, Delemont M (2004) Cyclic properties of superelastic shape memory alloy wires and bars. J Struct Eng 130(1):38–46. https://doi.org/10.1061/(ASCE)0733-9445(2004)130:1(38)

Elbahy YI, Youssef MA (2019) Flexural behaviour of superelastic shape memory alloy reinforced concrete beams during loading and unloading stages. Eng Struct 181:246–259. https://doi.org/10.1016/j.engstruct.2018.12.001

Fikri R, Dizhur D, Walsh K, Ingham J (2019) Seismic performance of reinforced concrete frame with masonry infill buildings in the 2010/2011 Canterbury, New Zealand earthquakes. Bull Earthq Eng 17(2):737–757. https://doi.org/10.1007/s10518-018-0476-8

Gharavi A, Asgarpoor M, Epackachi S (2022) Evaluation of plasticity-based concrete constitutive models under monotonic and cyclic loadings. Struct Des Tall Spec Build 31(6):e1919. https://doi.org/10.1002/tal.1919

Gurbuz T, Cengiz A (2025) Structural damages during the February 06, 2023 Kahramanmaraş earthquakes in Turkey. Soil Dyn Earthq Eng 191:109214. https://doi.org/10.1016/j.soildyn.2025.109214

Hallquist JO (2006) LS-DYNA theory manual. Livermore Software Technology Corporation, Livermore

Hosseini F, Gencturk B, Lahpour S, Gil DI (2015) An experimental investigation of innovative bridge columns with engineered cementitious composites and Cu–Al–Mn superelastic alloys. Smart Mater Struct 24(8):085029. https://doi.org/10.1088/0964-1726/24/8/085029

Hoult R, de Almeida JP (2022a) From experimental strain and crack distributions to plastic hinge lengths of RC walls with SMA rebars. Eng Struct 268:114731. https://doi.org/10.1016/j.engstruct.2022.114731

Hoult RD, de Almeida JP (2022b) Residual displacements of reinforced concrete walls detailed with conventional steel and shape memory alloy rebars. Eng Struct 256:114002. https://doi.org/10.1016/j.engstruct.2022.114002

Hwang H-J, Eom T-S, Park H-G (2015) Design considerations for interior RC beam–column joint with additional bars. Eng Struct 98:1–13. https://doi.org/10.1016/j.engstruct.2015.04.021

Ilia E, Mostofinejad D (2019) Seismic retrofit of reinforced concrete strong beam–weak column joints using EBROG method combined with CFRP anchorage system. Eng Struct 194:300–319. https://doi.org/10.1016/j.engstruct.2019.05.070

Kabir MR, Alam MS, Said AM, Ayad A (2016) Performance of hybrid reinforced concrete beam–column joint: a critical review. Fibers 4(2):13. https://doi.org/10.3390/fib4020013

Karayannis CG, Chalioris CE, Sirkelis GM (2008) Local retrofit of exterior RC beam–column joints using thin RC jackets—an experimental study. Earthq Eng Struct Dyn 37:727–746. https://doi.org/10.1002/eqe.783

Mohammadgholipour A, Billah AM (2023) Mechanical properties and constitutive models of shape memory alloy for structural engineering: a review. J Intell Mater Syst Struct 34(20):2335–2359. https://doi.org/10.1177/1045389X231185458

Mousavizadeh MM, Ghandi E, Farzam M, Gholizad A (2024) An experimental and numerical study of plastic hinge relocation in the exterior RC beam-to-column joints with the implementation of the local weakening method. Eng Struct 317:118696. https://doi.org/10.1016/j.engstruct.2024.118696

Nascimbene R (2013) An arbitrary cross section, locking free shear-flexible curved beam finite element. Int J Comput Methods Eng Sci Mech 14(2):90–103. https://doi.org/10.1080/15502287.2012.698706

Nascimbene R (2024) Investigation of seismic damage to existing buildings by using remotely observed images. Eng Fail Anal 161:108282. https://doi.org/10.1016/j.engfailanal.2024.108282
Nehdi M, Alam MS, Youssef MA (2010) Development of corrosion-free concrete beam–column joint with adequate seismic energy dissipation. Eng Struct 32(9):2518–2528. https://doi.org/10.1016/j.engstruct.2010.04.020
Oudah F, El-Hacha R (2017a) Plastic hinge relocation in concrete structures using the double-slotted-beam system. Bull Earthq Eng 15:2173–2199. https://doi.org/10.1007/s10518-016-0055-9
Oudah F, El-Hacha R (2017b) Joint performance in concrete beam–column connections reinforced using SMA smart material. Eng Struct 151:745–760. https://doi.org/10.1016/j.engstruct.2017.08.054
Oudah F, El-Hacha R (2018) Innovative self-centering concrete beam–column connection reinforced using shape memory alloy. ACI Struct J 115(3):777–790. https://doi.org/10.14359/51702132
Oudah F, El-Hacha R (2020) Monolithic SMA-reinforced double slotted beam–column connection. Smart Mater Struct 29(3):035002. https://doi.org/10.1088/1361-665X/ab62df
Pareek S, Suzuki Y, Araki Y, Youssef MA, Meshaly M (2018) Plastic hinge relocation in reinforced concrete beams using Cu–Al–Mn SMA bars. Eng Struct 175:765–775. https://doi.org/10.1016/j.engstruct.2018.08.072
Qian H, Li Z, Pei J, Kang L, Li H (2022) Seismic performance of self-centering beam–column joints reinforced with superelastic shape memory alloy bars and engineering cementitious composites materials. Compos Struct 294:115782. https://doi.org/10.1016/j.compstruct.2022.115782
Rutledge ST, Kowalsky MJ, Seracino R, Nau JM (2014) Repair of reinforced concrete bridge columns containing buckled and fractured reinforcement by plastic hinge relocation. J Bridge Eng 19(8):A4013001. https://doi.org/10.1061/(ASCE)BE.1943-5592.0000492
Saiidi MS, Wang H (2006) Exploratory study of seismic response of concrete columns with shape memory alloys reinforcement. ACI Mater J 103(3):436–443. https://doi.org/10.14359/15322
Saiidi MS, Sadrossadat-Zadeh M, Ayoub C, Itani A (2007) Pilot study of behavior of concrete beams reinforced with shape memory alloys. J Mater Civ Eng 19(6):454–461. https://doi.org/10.1061/(ASCE)0899-1561(2007)19:6(454)
Saiidi MS, O'Brien M, Sadrossadat-Zadeh M (2009) Cyclic response of concrete bridge columns using superelastic Nitinol and bendable concrete. ACI Struct J 106(1):69–77. https://doi.org/10.14359/56285
Sarkis AI, Sullivan TJ, Brunesi E, Nascimbene R (2022) Critical modelling criteria for precast pre-stressed hollow-core slabs. J Build Eng 54:104545. https://doi.org/10.1016/j.jobe.2022.104545
Sarkis AI, Sullivan TJ, Brunesi E, Nascimbene R (2023) Investigating the effect of bending on the seismic performance of hollow-core flooring. Int J Concr Struct Mater 17(1):18. https://doi.org/10.1186/s40069-023-00580-w
Shrestha KC, Araki Y, Nagae T, Koetaka Y, Suzuki Y, Omori T, Ishida K (2013) Feasibility of Cu–Al–Mn superelastic alloy bars as reinforcement elements in concrete beams. Smart Mater Struct 22(2):025025. https://doi.org/10.1088/0964-1726/22/2/025025
Tazarv M, Saiidi MS (2016) Low-damage precast columns for accelerated bridge construction in high seismic zones. J Bridge Eng 21(3):04015056. https://doi.org/10.1061/(ASCE)BE.1943-5592.0000806
Tolou Kian MJ, Cruz-Noguez C (2018) Reinforced concrete shear walls detailed with innovative materials: seismic performance. J Compos Constr 22(6):04018052. https://doi.org/10.1061/(ASCE)CC.1943-5614.0000893
Tsonos AG (2005) Cyclic load behaviour of reinforced concrete beam–column subassemblages of modern structures. WIT Trans Built Environ 81:1–10. https://doi.org/10.14359/18777
Youssef MA, Alam MS, Nehdi M (2008) Experimental investigation on the seismic behavior of beam–column joints reinforced with superelastic shape memory alloys. J Earthq Eng 12(7):1205–1222. https://doi.org/10.1080/13632460802003082